Active control of the free surface of a rivulet of a nematic liquid crystal with an electric field

Akhshay S. Bhadwal,[1,*] Joseph R. L. Cousins,[2,3,*] Nigel J. Mottram,[2] Stephen K. Wilson,[3] Brian R. Duffy,[3] Ian C. Sage,[1] and Carl V. Brown[1,†]

[1]*SOFT Group, Department of Physics and Mathematics, School of Science and Technology, Nottingham Trent University, Clifton Lane, Nottingham NG11 8NS, United Kingdom*

[2]*School of Mathematics and Statistics, University of Glasgow, University Place, Glasgow G12 8QQ, United Kingdom*

[3]*Department of Mathematics and Statistics, University of Strathclyde, Livingstone Tower, 26 Richmond Street, Glasgow G1 1XH, United Kingdom*

(Received 10 May 2023; accepted 10 May 2024; published 24 June 2024)

Active control of a rivulet of a nematic liquid crystal is achieved by local modification of the effective viscosity with an applied electric field. Specifically, using the nematic 5CB, control of the free surface of the rivulet is achieved through manipulation of the effective viscosity induced by the competition of moments due to viscous shear stress alignment and electric field alignment. The experimentally observed dependencies of the rivulet height on the volume flux and the strength of the applied electric field are successfully captured by a theoretical model based on the Ericksen-Leslie equations.

DOI: 10.1103/PhysRevFluids.9.064002

I. INTRODUCTION

The controlled manipulation of the free surface of a rivulet at micron and millimeter scales plays an important role in many industrial and technological applications. Examples range from industrial coating processes [1] to recently developed open microfluidic-based laboratory-on-a-chip platforms [2,3], microelectronic cooling systems [4], and biomedical devices [5]. Moreover, active control and manipulation of free surfaces can also advance the understanding of physical effects (e.g., meandering instabilities in rivulet flow [6–8]), possibly allowing the investigation of otherwise inaccessible unstable free surfaces. Non-Newtonian rivulets are often studied under isothermal conditions (e.g., theoretical studies of classical non-Newtonian fluids, such as power-law fluids [9–12], Herschel-Bulkley fluids [13], generalized Newtonian fluids [14], and viscoelastic fluids [15]); however, thermal effects play a key role in many real-world situations, such as manufacturing [16,17] and geophysics [18]. Experimental [19] and theoretical [20,21] studies have examined temperature-dependent viscosity effects; however, temperature-dependent control remains difficult due to slow response times, environmental temperature fluctuations, and changes to the physical properties of the liquid being studied.

*These authors contributed equally to this work.
†Contact author: carl.brown@ntu.ac.uk

In the present work, we show that active control of the free surface of a rivulet of nematic liquid crystal can be achieved by local modification of the effective viscosity with an applied electric field. Specifically, control of the free surface is achieved through manipulation of the effective viscosity induced by the competition of moments due to viscous shear stress alignment and electric field alignment. Electric-field-induced changes to the local viscosity of a nematic occur upon application of an electric field due to the reorientation of the average molecular orientation, termed the director, and the director-orientation dependence of the nematic viscosity [22,23]. This orientation dependence of the viscosity is parametrized by four Miesiowicz viscosities: η_1 when the director is aligned in the flow direction; η_2 when the director is aligned in the shear gradient direction; the isotropic viscosity η_3 when the director is aligned perpendicular to both the flow direction and the shear gradient direction; and the viscosity η_{12} that plays a role when the director is aligned in any direction that is not one of the three fundamental directions mentioned previously. Under the influence of a shear gradient, the director aligns at a specific angle to the flow direction, called the Leslie angle and denoted by θ_{L}, and the corresponding effective viscosity is denoted by η_{L} [23]. It is the competition between the electric field and flow-aligning effects that provides controllability of the effective viscosity, which in turn provides controllability of the free surface of the rivulet. In our experiments, we use the nematic 4-cyano-4-pentylbiphenyl (CAS 40817-08-1), henceforth referred to by its common name of "5CB," which has orientation-dependent effective viscosity, and show that significant changes in the effective viscosity can be created in a localized region of the flow under isothermal conditions while keeping the other physical properties of the liquid constant.

II. EXPERIMENTAL PROCEDURE

Experimentally we observed the flow of a straight-sided pinned nematic rivulet of 5CB on a borosilicate transparent glass substrate of dimensions 75 mm × 25 mm in the $\hat{\boldsymbol{x}}$ and $\hat{\boldsymbol{y}}$ axes inclined at an angle $\alpha = 25^{\circ}$ to the horizontal with the $\hat{\boldsymbol{z}}$ axis normal to the substrate located at $z = 0$, as shown in Fig. 1.

The substrate was coated with a transparent conducting indium tin oxide layer (ITO; 75 nm thickness and 75 Ω/sq resistivity), creating a continuous ITO electrode on the substrate. A second borosilicate transparent glass substrate was positioned at $z = H$ and was coated with an identical conducting ITO layer in a rectangular patch of dimensions 15 mm × 25 mm. The two substrates, henceforth referred to as the lower and upper substrates, were separated by a polymeric spacer of thickness $H = 1.1$ mm to ensure an air gap from the free surface to the upper substrate. A wetting strip of constant semiwidth a ($2a = 1.8$ mm) was created on the lower substrate, causing the rivulet to have pinned contact lines at $y = \pm a$. The strip comprised a self-assembled monolayer of OTS [trichloro(octyl) silane; CAS 5283-66-9] which provides a moderately low surface energy, surrounded by a self-assembled monolayer of PFOCTS (trichloro[1H,1H,2H,2H-perfluorooctyl] silane; CAS 78560-45-9) which provides a very low surface energy and therefore resists wetting by the 5CB. A constant volume flux Q of 5CB was established in the x direction on the wetting strip using a flow microcontroller, creating a rivulet of 5CB. The air–5CB free surface has previously been shown to have homeotropic preferred alignment [24], i.e., a preferred alignment normal to the free surface. Additionally, the wetting strip was also shown to have homeotropic preferred alignment by observing a static droplet of 5CB on the wetting strip under crossed polarizers. A high-frequency ac sine-wave voltage V_{ac} ($f = 10$ kHz; rms voltage henceforth denoted V) was applied between the ITO electrodes using a waveform generator connected to a voltage amplifier, which produced an electric field $\boldsymbol{E}$ in the z direction. A high-frequency ac (rather than a dc) voltage was used to avoid shielding by mobile ionic species that are inevitably present in the nematic, and thus ensure full penetration of the electric field into the rivulet [25].

Experimental images of a top view and a side view of the rivulet were recorded using two CMOS cameras. Specifically, as shown in Fig. 1, the top-view camera (fitted with a 10× objective lens) imaged the rivulet in the z direction and the side-view camera (fitted with a 5× objective lens) imaged the rivulet in the y direction.

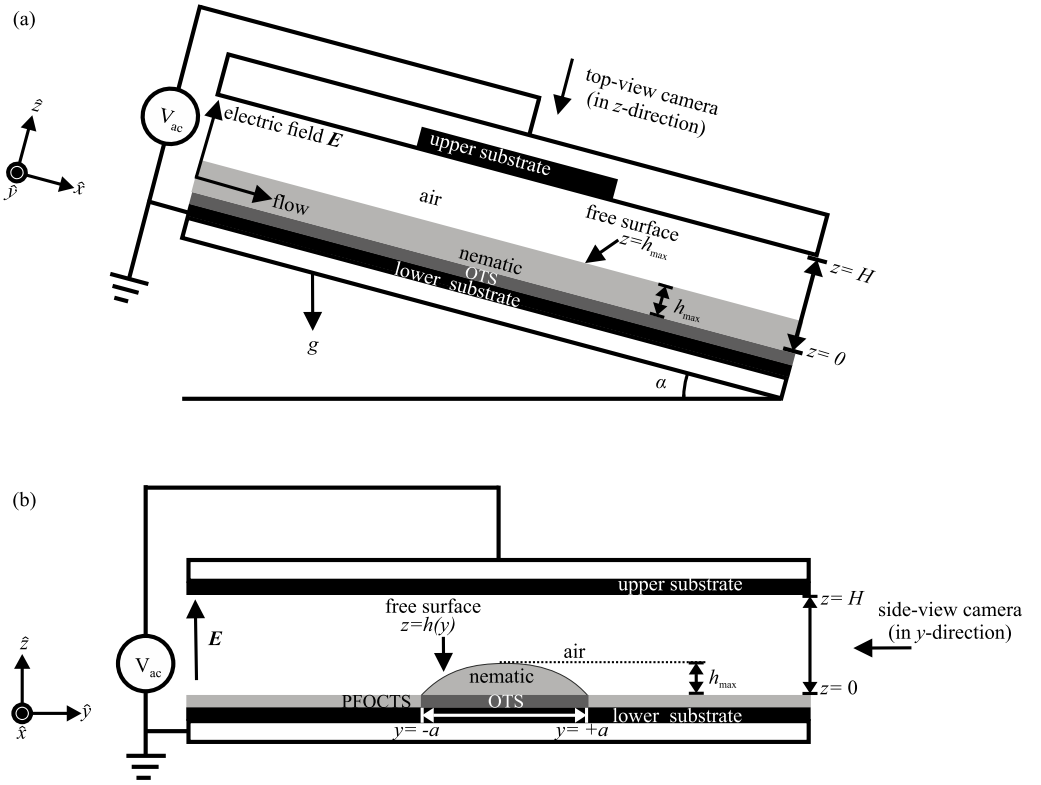

FIG. 1. (a) A side view and (b) a front view of a straight-sided pinned nematic rivulet of 5CB on a substrate inclined at an angle α to the horizontal. The lower substrate is coated with a continuous ITO electrode at $z = 0$ with electric potential $U = 0$, the upper substrate is coated with a rectangular patch ITO electrode at $z = H$ with electric potential $U = V$, and the applied ac sine-wave voltage V_{ac} produces the electric field $\boldsymbol{E}$. The front view shows the wetting strip of constant semiwidth a on the lower substrate consisting of a strip of moderately low surface energy OTS surrounded by very low surface energy PFOCTS. The $\hat{\boldsymbol{x}}$, $\hat{\boldsymbol{y}}$, and $\hat{\boldsymbol{z}}$ axes, the free surface of the rivulet $z = h(y)$, and the maximum height of the free surface h_{max} are also shown.

The unavoidable degradation and contamination of the wetting strip, resulting in overspill at its straight edges, necessitated regular device disassembly and reassembly between sets of measurements. The best tolerances of the values of a, α, and H (including the cell uniformity) that could be obtained was $2a = 1.80 \pm 0.09$ mm, $\alpha = 25.0 \pm 1.3^\circ$, and $H = 1.10 \pm 0.11$ mm.

After an initial transient, the maximum height of the free surface, henceforth denoted h_{max}, attained a constant value that depends upon the value of Q. Experimental images of the rivulet under different combinations of the volume flux ($Q = 250$, 500, and 1000 nL s^{-1}) and the voltage ($V = 0$ V and $V = 1000$ V) are shown in Figs. 2(a) and 2(b), respectively. In particular, the values of the fluid velocity at the centerline of the free surface, where the maximum velocity within the rivulet occurs, denoted by u_{max}, are shown and indicated by the white arrows. This velocity was determined by tracking the movement of dust particles moving down the centerline of the rivulet using a particle imaging velocimetry technique. Note that the lighter white stripe that is visible in the side view of the rivulet for $Q = 1000$ nL s^{-1} is an optical artifact due to the refraction of the edge of the substrate that lies between the rivulet and the light source. The variation in the maximum height of the free surface h_{max} was analyzed using MATLAB and IMAGEJ [26,27].

In the absence of the applied voltage (i.e., when $V = 0$ V), the moments due to viscous shear stress produce the well-known flow-alignment behavior [23], as indicated in Fig. 2(c), which shows

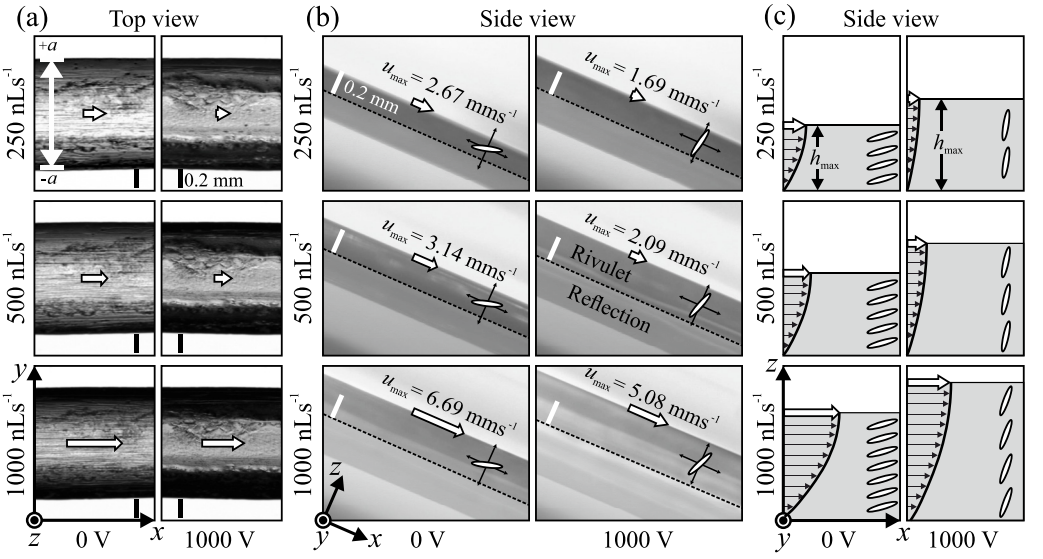

FIG. 2. Experimental images of (a) a top view and (b) a side view of the rivulet under different combinations of the volume flux ($Q = 250$, 500, and 1000 nL s^{-1}) and the voltage ($V = 0$ V and $V = 1000$ V). In (a) the white bidirectional arrow shows the width of the rivulet and the end bars indicate the positions of the pinned contact lines at $y = \pm a$. In (b) the rivulet is above the dashed black line and its reflection in the lower substrate is below it, as labeled in the $Q = 500$ nL s^{-1} with $V = 1000$ V panel, and the values of u_{max} are shown. (c) A schematic diagram of a side view of a representative director profile (white ellipsoids) and fluid velocity (solid black arrows) along the centerline of the rivulet ($y = 0$) under different combinations of the volume flux ($Q = 250$, 500, and 1000 nL s^{-1}) and the voltage ($V = 0$ V and $V = 1000$ V). The fluid velocity at the centerline of the free surface, where the maximum velocity within the rivulet occurs, is shown by the white arrows in (a) and (b). A scale bar of 0.2 mm is shown with a black bar in each image of (a) and with a white bar in each image of (b).

a schematic diagram of a side view of a representative director profile (white ellipsoids) and fluid velocity (solid black arrows) along the centerline of the rivulet ($y = 0$).

In the presence of the applied voltage (specifically for 0 V $< V \leqslant 1000$ V in the present experiments), since 5CB has a positive dielectric anisotropy $\Delta\epsilon = 11.5$ [23], the moments due to electric field alignment act to align the director parallel to the $\hat{z}$ axis in the bulk of the rivulet. As mentioned in Sec. I, the effective viscosity of the rivulet when the director is aligned at the Leslie angle is given by η_L, and the effective viscosity of the rivulet when the director is aligned in the shear gradient direction (i.e., parallel to the $\hat{z}$ axis) is given by η_2, which is larger than η_L [28], and hence the presence of the applied electric field increases the effective viscosity of the rivulet. Specifically, the application of the voltage to the system creates competition between the moments due to viscous shear stress alignment and electric field alignment that increases the effective viscosity of the rivulet, decreasing the fluid velocity, and hence leading to an increase in the maximum height of the free surface of the rivulet, as shown in Fig. 2(b) and also indicated in Fig. 2(c).

III. THEORETICAL MODEL

In order to model and further understand the dependence of the height of the free surface of the rivulet on the problem parameters theoretically, we employ the well-established Ericksen-Leslie theory for the nematic, within which the average molecular orientation is described by the nematic director $\boldsymbol{n}$, and Gauss' law for the electric potential [23]. Motivated by the experimental setup, we assume that the rivulet is uniform in the x direction, and hence that the system is

described by the height of the free surface $z = h(y)$ of the rivulet, the nematic director $\boldsymbol{n}(y, z) = \cos\theta(y, z)\cos\phi(y, z)\hat{\boldsymbol{x}} + \cos\theta(y, z)\sin\phi(y, z)\hat{\boldsymbol{y}} + \sin\theta(y, z)\hat{\boldsymbol{z}}$, where θ is the angle between $\boldsymbol{n}$ and the xy plane and ϕ is the angle between the projection of $\boldsymbol{n}$ onto the xy plane and the $\hat{\boldsymbol{x}}$ axis, the electric potential $U(y, z)$, the fluid velocity $\boldsymbol{u}(y, z) = u(y, z)\hat{\boldsymbol{x}} + v(y, z)\hat{\boldsymbol{y}} + w(y, z)\hat{\boldsymbol{z}}$, and the effective pressure $\tilde{p}(y, z) = p_a + p(y, z) + \omega(\boldsymbol{n}, U)$, where p_a is the constant atmospheric pressure, p is the usual fluid pressure minus atmospheric pressure, and ω is the free-energy density [23]. The director angles θ and ϕ are often termed the tilt and twist angles, respectively. No-slip and no-penetration conditions are assumed at the substrate, as well as normal and tangential stress balances and the kinematic condition at the free surface. The contact lines are assumed to be pinned at $y = \pm a$. Together with the prescribed electric potentials at the lower and upper electrodes, $U = 0$ and $U = V$, respectively, we assume continuity of the electric potential and of the normal component of the electric displacement field at the free surface. As mentioned in Sec. I, the Miesowicz viscosities of the nematic are denoted by η_1, η_2, η_3 (the isotropic viscosity) and η_{12} and its rotational and torsional viscosities by γ_1 and $\gamma_2 = \eta_1 - \eta_2$ [23].

Since the transverse (i.e., the z-y) aspect ratio of the rivulet is small in the experiments, we use the standard lubrication approximation for a thin rivulet with prescribed volume flux [29–31], and nondimensionalize the governing equations so that y, z, u, v, w, p, and U are scaled with l, δl, $\mathcal{U}$, $\mathcal{V}$, $\mathcal{W}$, $\mathcal{P}$, and V, respectively, where $l = [\sigma/(\rho g)]^{1/2}$ is the capillary length, $\delta = [\eta_3 Q/(\rho g l^4)]^{1/3} \ll 1$ is the aspect ratio, $\mathcal{U} = \rho g\delta^2 l^2/\eta_3$, $\mathcal{V} = \rho g\delta^3 l^2/\eta_3$ and $\mathcal{W} = \rho g\delta^4 l^2/\eta_3$ are velocity scales, $\mathcal{P} = \rho g l\delta$ is the pressure scale, σ is the constant surface tension, ρ is the constant fluid density, and g is the magnitude of acceleration due to gravity. All viscosities are nondimensionalized with the isotropic viscosity η_3. The lubrication approximation has been used with considerable success in a wide variety of both Newtonian and non-Newtonian thin-film flow problems [1,32]. Experimental values of the viscosity $\eta_3 = 0.0326$ Pa s, volume flux $Q = 250$–1000 nL s^{-1}, capillary length $l = 1.8$ mm, and elastic constant $K = 6.2$–8.2 pN lead to an Ericksen number of $\mathrm{Er} = \eta_3 Q/(lK) \approx 550$–$2900 \gg 1$, and so elastic effects can be safely neglected. Our recent work [24,33] shows that the effects of nematic anchoring (due to the anisotropic component of the nematic surface energy) are also negligible as the anchoring strength of 5CB is around four orders of magnitude weaker than nematic surface tension (due to the isotropic component of the nematic surface energy). With the above scalings and with elastic and anchoring effects neglected, the leading-order component of angular momentum out of the shear (i.e., the x-z) plane of the flow is zero, and so $\phi \equiv 0$, and the director tilt angle θ is determined by the balance of moments due to viscous shear stress alignment and electric field alignment. In order to simplify the model further, we use the fact that two nondimensional effective viscosities that appear in the full Ericksen-Leslie equations, i.e., $\eta_1 + \eta_2 - 2\eta_3 - \gamma_1$ and $3\eta_1 + \eta_2 - 4\eta_3 - \gamma_1 + 2\eta_{12}\sin^2\theta$, are small for 5CB for all values of θ, and therefore we set them both to zero. As we shall see, the experimental and theoretical results show good agreement despite the above assumptions.

With the above assumptions, the nondimensional leading-order conservation of mass equation and linear momentum equations are a generalization of the standard equations for a thin Newtonian rivulet [29–31], and are given by

$$0 = v_y + w_z, \tag{1}$$

$$0 = \sin\alpha + [\mu_1(\theta)u_z]_z, \quad 0 = -\tilde{p}_y + [\mu_2(\theta)v_z]_z, \quad 0 = -\cos\alpha - \tilde{p}_z, \tag{2}$$

where

$$\mu_1(\theta) = \eta_1\cos^2\theta + \eta_2\sin^2\theta + \eta_{12}\sin^2\theta\cos^2\theta \quad \text{and} \quad \mu_2(\theta) = \eta_2\sin^2\theta + \eta_3\cos^2\theta \tag{3}$$

are effective viscosities. The nondimensional leading-order angular momentum equation is given by

$$0 = m(\theta)u_z + \frac{\epsilon_0\Delta\epsilon l V^2}{2\eta_3 Q}\sin 2\theta U_z^2, \tag{4}$$

where $m(\theta) = (\gamma_1 + \gamma_2 \cos 2\theta)/2$ is an effective viscosity, and the nondimensional leading-order equations for the electric potential are

$$0 = [\epsilon(\theta)\, U_z]_z \quad \text{for} \quad 0 \leqslant z \leqslant h \quad \text{and} \quad 0 = U_{zz} \quad \text{for} \quad h \leqslant z \leqslant H, \tag{5}$$

where $\epsilon(\theta) = \epsilon_\perp + \Delta\epsilon \sin^2\theta$ and ϵ_0, $\epsilon_\perp$, and $\Delta\epsilon$ are the permittivity of free space, the dielectric permittivity perpendicular to the director, and the dielectric anisotropy, respectively [23]. The electric potential gradient U_z can readily be found by solving the equations for the electric potential subject to the relevant boundary conditions. We now assume that the tilt angle θ can be approximated by its depth-averaged value, so that

$$\theta(y, z) \approx \hat{\theta}(y) = \frac{1}{h}\int_0^h \theta(y, z)\mathrm{d}z, \tag{6}$$

and then integrate (4) between $z = 0$ and $z = h(y)$. Solving the conservation of mass equation (1) and linear momentum equations (2) subject to the relevant boundary conditions then yields

$$u = \frac{\sin\alpha}{2\mu_1(\hat{\theta})}(2h - z)z, \quad v = 0, \quad w = 0, \tag{7}$$

$$p = -\frac{\partial^2 h}{\partial y^2} + \cos\alpha(h - z), \tag{8}$$

$$h = \left[\int_{-a}^{+a} \frac{\sin\alpha}{3\mu_1(\hat{\theta})}\left(\frac{\cosh(ka) - \cosh(ky)}{k\sinh(ka)}\right)^3 \mathrm{d}y\right]^{-1/3} \frac{\cosh(ka) - \cosh(ky)}{k\sinh(ka)}, \tag{9}$$

$$0 = \frac{m(\hat{\theta})}{\mu_1(\hat{\theta})}h + \frac{\epsilon_0\,\Delta\epsilon l V^2}{\sin\alpha\,\eta_3 Q}\frac{\sin 2\hat{\theta}}{[\epsilon(\hat{\theta})(H - h) + h]^2} \tag{10}$$

for $0 < \alpha \leqslant \pi/2$, where $k = (\cos\alpha)^{1/2}$, and $\hat{\theta}$ is the depth-averaged tilt angle given by (6). The height of the free surface of the rivulet (9) takes the same functional form as that of a thin Newtonian rivulet [29–31] with the balance of moments due to viscous shear stress alignment and electric field alignment determining the effective rivulet viscosity $\mu_1(\hat{\theta})$. Electrically controlling the effective rivulet viscosity $\mu_1(\hat{\theta})$ can, therefore, give rise to changes in the height of the rivulet. For given material and given geometric parameters, the free surface $h(y)$ and the depth-averaged tilt angle $\hat{\theta}(y)$ can be determined using standard quadrature and root-finding numerical methods from the coupled integro-algebraic equations (9) and (10).

As mentioned above, the experimental results can be interpreted in terms of the balance of moments due to viscous shear stress alignment and electric field alignment in the system. In particular, in the absence of the applied voltage, only viscous shear stress alignment occurs, (10) reduces to $m(\hat{\theta}) = 0$, and the nematic exhibits the well-known flow-alignment behavior [23] with $\hat{\theta} = \theta_\mathrm{L}$ and effective viscosity $\mu_1(\theta_\mathrm{L}) = \eta_\mathrm{L} \approx 0.024$ Pa s, where θ_L is the Leslie angle, as shown in Fig. 2(c) for $V = 0$ V. In this special case (9) reduces to the explicit expression for the height of a thin rivulet of a Newtonian fluid with viscosity η_L, namely,

$$h = \left(\frac{9\eta_\mathrm{L}\cos^2\alpha}{f(ka)\sin\alpha}\right)^{1/3}\frac{\cosh(ka) - \cosh(ky)}{k\sinh(ka)}, \tag{11}$$

where

$$f(ka) = 15ka\coth^3(ka) - 15\coth^2(ka) - 9ka\coth(ka) + 4 \tag{12}$$

for $0 < \alpha \leqslant \pi/2$. However, in the presence of the applied voltage, the field acts to align the nematic in the z direction, and the balance of moments gives a fixed director $\hat{\theta}$ and effective viscosity $\mu_1(\hat{\theta}) > \eta_\mathrm{L}$, as shown in Fig. 2(c) for $V = 1000$ V. In the limit in which the electric field alignment is dominant, $V \to \infty$, (10) reduces to $\hat{\theta} = \pi/2$, and the director aligns completely

with the field with effective viscosity $\mu_1(\pi/2) = \eta_2 \approx 0.105$ Pa s. In this limit (9) reduces to the explicit expression for the height of a thin rivulet of a Newtonian fluid with viscosity η_2 given by (11) with η_L replaced by η_2. Since, as noted previously, $\eta_2 > \eta_L$, the maximum value of h_{max} occurs in this limit. The maximum difference in viscosity that can be obtained using this system is $\Delta\eta = \eta_2 - \eta_L \approx 0.081$ Pa s, i.e., an increase of more than three times the original value. It is also clear that the extent to which $\hat{\theta}$ approaches the Leslie angle θ_L increases with the magnitude of Q, but we find that the change in $\mu_1(\hat{\theta})$ due to this is negligible in the absence of the applied voltage. However, there is, of course, a significant change in h_{max} induced by an increasing flow rate due to the conservation of volume, as shown in Fig. 2(b).

IV. RESULTS AND DISCUSSION

In order to quantify the success of the model in describing the competition between moments due to viscous shear stress alignment and electric field alignment, we varied the applied voltage for three volume fluxes: $Q = 250$ nL s^{-1}, $Q = 500$ nL s^{-1}, and $Q = 1000$ nL s^{-1}. Solving the coupled integro-algebraic equations (9) and (10) using the parameter values for 5CB ($\rho = 1020$ kg m^{-3}, $g = 9.81$ m s^{-2}, $\sigma = 0.0326$ N m^{-1}, $\eta_1 = 0.0204$ Pa s, $\eta_2 = 0.1052$ Pa s, $\eta_3 = 0.0326$ Pa s, $\eta_{12} = -0.0060$ Pa s, and $\gamma_1 = 0.0777$ Pa s) enables us to calculate h_{max} for the volume fluxes and applied voltages used in these experiments.

Figures 3(a) and 3(b) show a comparison of the experimental results and the values predicted by the theoretical model for h_{max} for a range of values of V and Q. Figure 3(a) shows a comparison of the experimental results (data points) and the values predicted by the theoretical model (lines) for h_{max} for $Q = 250$ nL s^{-1} (closed squares and dotted lines), $Q = 500$ nL s^{-1} (closed diamonds and dashed lines), and $Q = 1000$ nL s^{-1} (closed circles and solid lines) as the applied voltage is varied from $V = 0$ V to $V = 1000$ V. Figure 3(a) also includes the region of h_{max} values predicted by the theoretical model taking into account the tolerances of the values of a, α, and H mentioned earlier. Figure 3(a) shows that as the applied voltage is increased, the maximum height of the free surface h_{max} increases, with the experiments and the theoretical model in qualitative agreement. In the absence of the applied voltage, the increase in value of h_{max} for increasing values of Q is due to the conservation of volume, i.e., as the value of Q increases, more liquid is being fed into the rivulet, and since the rivulet is pinned in the y direction, h_{max} increases. In the presence of the applied voltage, the effective viscosity of the rivulet increases, decreasing the fluid velocity, and hence leading to an increase in the height of the free surface. The change in the effective viscosity is quantified in Figs. 3(c) and 3(d), which show the minimum value of $\mu_1[\hat{\theta}(y)]$ across the width of the rivulet predicted by the theoretical model, denoted by $\mu_{1min} = \mu_1[\hat{\theta}(0)]$, for the same range of values of V and Q as used in Figs. 3(a) and 3(b), respectively. In particular, the results shown in Figs. 3(c) and 3(d) show that the presence of an applied voltage $V = 1000$ V substantially increases the effective viscosity of the rivulet, but that the effective viscosity is only weakly dependent on the value of Q.

Evidently, in Fig. 3(a) for the voltage range $0\text{ V} < V \leqslant 400$ V, the experimentally measured values of h_{max} exceed the predictions of the model. One possible cause of this is the presence of moving defects, which are elongated along the direction of the flow. These defects are evident in the enhanced experimental images shown in Fig. 4, which were generated from the same original images as used to create Fig. 2(a) by removing the static backgrounds and enhancing visibility of the defects by image processing. Specifically, the image processing was performed by calculating the difference between two consecutive frames of the video and then applying morphological processing and filtering using MATLAB [26]. In particular, Fig. 4 shows that the number of defects increases as Q increases, as has been previously reported [34], and, due the annealing of defects by the applied electric field, the number of defects reduces as V increases. Defects can act as localized isotropic regions in the nematic with effective viscosity η_3, for which $\eta_L < \eta_3 < \eta_2$. As previously discussed, in the absence of the applied voltage, the effective viscosity of the rivulet is η_L and, therefore, the presence of defects produces an increase in the effective viscosity of the rivulet, increasing the

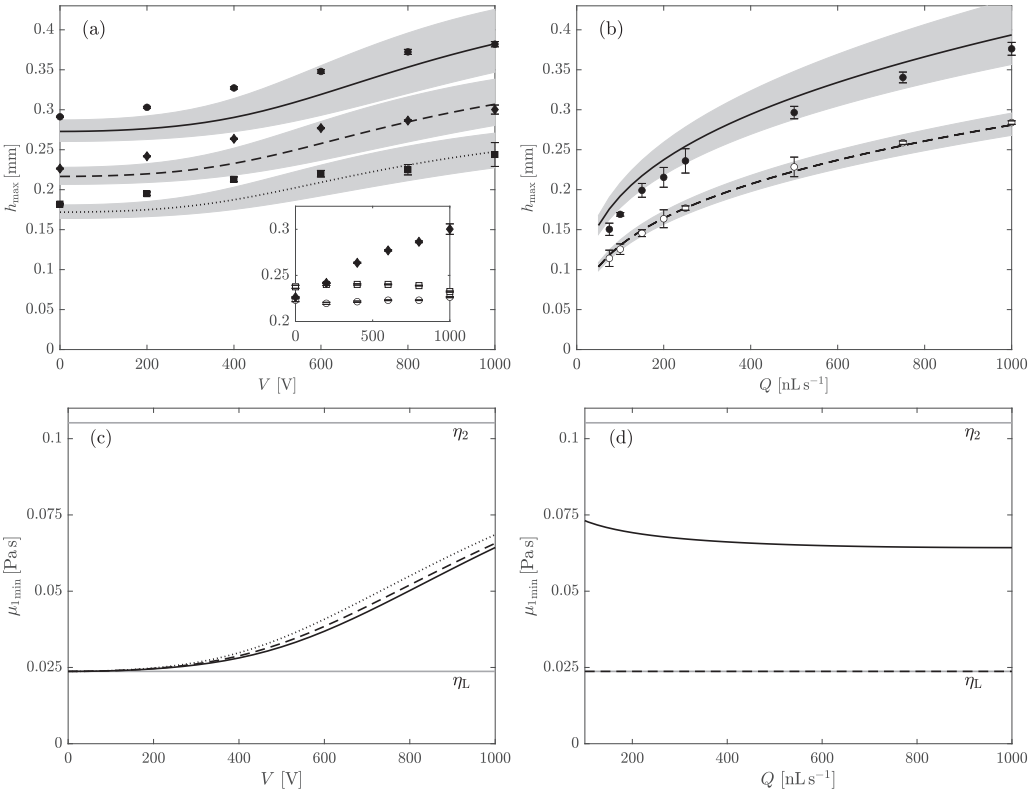

FIG. 3. Experimental results (data points) and the values predicted by the theoretical model (lines) for the maximum height of the free surface h_{max} (a) plotted as a function of the applied voltage V for $Q = 250$ nL s^{-1} (closed squares and dotted line), $Q = 500$ nL s^{-1} (closed diamonds and dashed line), and $Q = 1000$ nL s^{-1} (closed circles and solid line) and (b) plotted as a function of the prescribed flux Q for $V = 0$ V (open circles and dashed line) and $V = 1000$ V (closed circles and solid line). The inset in (a) shows the experimental values of h_{max} for $Q = 500$ nL s^{-1} (closed diamonds) and the results of control experiments with propylene glycol (open black circles) at $Q = 275$ nL s^{-1} and LCT 07-1132 (open black squares) at $Q = 500$ nL s^{-1}. The gray regions in both (a) and (b) represent the region of h_{max} values predicted by the theoretical model taking into account the tolerances of the values of a, α, and H given in the text. The minimum value of $\mu_1[\hat{\theta}(y)]$ across the width of the rivulet predicted by the theoretical model $\mu_{1min} = \mu_1[\hat{\theta}(0)]$ (c) plotted as a function of the applied voltage V for $Q = 250$ nL s^{-1} (dotted line), $Q = 500$ nL s^{-1} (dashed line), and $Q = 1000$ nL s^{-1} (solid line) and (d) plotted as a function of the prescribed flux Q for $V = 0$ V (dashed line) and $V = 1000$ V (solid line). The gray horizontal lines in both (c) and (d) indicate the values of η_L and η_2.

experimental value of h_{max}. However, we note that this defect-induced effect is expected to be less important at low voltages since $\eta_3 \sim \eta_L$ for the parameter values of 5CB [28], which is consistent with the good agreement at $V = 0$ V. At intermediate voltages, the effective viscosity of the rivulet is determined by the balance of moments due to viscous shear stress alignment and electric field alignment, resulting in a value in a range of effective viscosities from η_L to η_2, and the effects of the defects are hard to discern. At high voltages, there is a noticeable decrease in the number of defects observed in comparison to the number in the absence of the applied voltage (see the experimental images shown in Fig. 2(a) for $V = 1000$ V). The density of defects has previously been shown to decrease in the presence of the electric fields [35,36], perhaps explaining the improved agreement for high voltages.

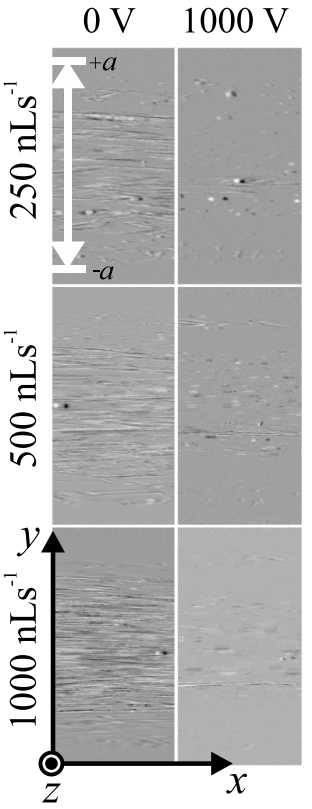

FIG. 4. Enhanced experimental images of a top view of the rivulet under different combinations of the volume flux ($Q = 250$, 500, and 1000 nL s^{-1}) and the voltage ($V = 0$ V and $V = 1000$ V). The white bidirectional arrow shows the width of the rivulet and the end bars indicate the positions of the pinned contact lines at $y = \pm a$.

In order to confirm that the increase in free surface height is not due to other effects, for instance, electrostatic effects, such as dielectrophoresis [37,38], we performed control experiments. Specifically, we used the same device and rivulet width, and adjusted Q to give similar $h_{\max}$ values to the 5CB rivulet when the voltages $V = 0$ V and $V = 1000$ V are applied, but with different liquids. One control experiment used a high-permittivity isotropic liquid, namely, propylene glycol (isotropic permittivity $\epsilon = 35$) [38], which due to its high permittivity will show if dielectrophoresis effects are significant in the system, while the other used a negative dielectric anisotropy nematic liquid crystal material, namely, LCT 07-1132 ($\Delta\epsilon = -3.44$) [35], which due to its negative dielectric anisotropy will induce a much smaller change in viscosity (namely, from η_{L} to η_1) in response to the electric field and therefore allows us to discern if any other effects are present. As shown in the inset in Fig. 3(a), neither control experiment showed an increase in $h_{\max}$ in the presence of the applied voltage, which is consistent with our conclusion that the increase in free surface height is not due to electrostatic effects [37,38].

Given the quantitative success of the model at $V = 0$ V and $V = 1000$ V, we consider the variation of $h_{\max}$ with increasing values of the volume flux Q for the voltages $V = 0$ V and $V = 1000$ V. Figure 3(b) shows a comparison of the experimental results (data points) and the values predicted by the theoretical model (lines) for $h_{\max}$ at $V = 0$ V (open circles and dashed lines) and $V = 1000$ V (closed circles and solid lines) when the volume flux Q was quasistatically increased from 75 to 1000 nL s^{-1} for a rivulet with semiwidth of $2a = 1.65 \pm 0.08$ mm. In order to achieve this change

quasistatically, we allowed for sufficient settling time so that transient changes in the profile $h_{\max}$ (of between 10 and 25 s) were accounted for and the rivulet had reached equilibrium. Again, as in Fig. 3(a), Fig. 3(b) also includes the region of $h_{\max}$ values predicted by the theoretical model taking into account the tolerances of the values of a, α, and H mentioned earlier. In the absence of the applied voltage $V = 0$ V and in the presence of a high voltage $V = 1000$ V, good quantitative agreement is found between the predictions of the theoretical model and the experimental data.

V. CONCLUSIONS

In summary, we have demonstrated, both experimentally and theoretically, active control of the free surface of a rivulet of nematic liquid crystal by local modification of the effective viscosity with an applied electric field rather than, for instance, electrostatic, dielectrophoretic, or thermal effects. Control of the free surface was achieved through manipulation of the effective viscosity induced by the competition of moments due to viscous shear stress alignment and electric field alignment. The success of this approach opens up possibilities for controlling free surfaces, offering a promising approach for providing insights into the behavior of reconfigurable free-surface microfluidic laboratory-on-chip applications. For example, a simple modification of the present experimental system could be used to study a pinned rivulet with spatially varying width or prescribed meanders, either of which would enable an investigation of the effects of *in situ* viscosity changes on the free surface shape at various positions along the rivulet.

All data supporting this work are provided at [39].

ACKNOWLEDGMENTS

The authors would like to acknowledge the financial support of the Engineering and Physical Sciences Research Council (EPSRC) via EPSRC Research Grants No. EP/T012986/1 and No. EP/T012501/2. We also wish to thank Russell Metcalfe (Nottingham Trent University) for his technical support with the experiments, and Professor Martin Bencsik (also Nottingham Trent University) for assistance with the image processing used to create Fig. 4.

[1] A. Oron, S. H. Davis, and S. G. Bankoff, Long-scale evolution of thin liquid films, Rev. Mod. Phys. **69**, 931 (1997).

[2] P. Kolliopoulos and S. Kumar, Capillary flow of liquids in open microchannels: Overview and recent advances, npj Microgr. **7**, 51 (2021).

[3] A. Olanrewaju, M. Beaugrand, M. Yafia, and D. Juncker, Capillary microfluidics in microchannels: From microfluidic networks to capillaric circuits, Lab Chip **18**, 2323 (2018).

[4] B. Schilder and P. Stephan, Design and operation of a novel capillary pumped two-loop system for cooling of electronic devices, Heat Transfer Eng. **33**, 12 (2012).

[5] N. M. Oliveira, S. Vilabril, M. B. Oliveira, R. L. Reis, and J. F. Mano, Recent advances on open fluidic systems for biomedical applications: A review, Mater. Sci. Eng. C **97**, 851 (2019).

[6] N. Le Grand-Piteira, A. Daerr, and L. Limat, Meandering rivulets on a plane: A simple balance between inertia and capillarity, Phys. Rev. Lett. **96**, 254503 (2006).

[7] B. Birnir, K. Mertens, V. Putkaradze, and P. Vorobieff, Meandering fluid streams in the presence of flow-rate fluctuations, Phys. Rev. Lett. **101**, 114501 (2008).

[8] A. Daerr, J. Eggers, L. Limat, and N. Valade, General mechanism for the meandering instability of rivulets of Newtonian fluids, Phys. Rev. Lett. **106**, 184501 (2011).

[9] S. K. Wilson, B. R. Duffy, and R. Hunt, A slender rivulet of a power-law fluid driven by either gravity or a constant shear stress at the free surface, Q. J. Mech. Appl. Math. **55**, 385 (2002).

[10] Y. M. Yatim, S. K. Wilson, and B. R. Duffy, Unsteady gravity-driven slender rivulets of a power-law fluid, J. Non-Newtonian Fluid Mech. **165**, 1423 (2010).
[11] F. H. H. Al Mukahal, B. R. Duffy, and S. K. Wilson, A rivulet of a power-law fluid with constant contact angle draining down a slowly varying substrate, Phys. Fluids **27**, 052101 (2015).
[12] F. H. H. Al Mukahal, S. K. Wilson, and B. R. Duffy, A rivulet of a power-law fluid with constant width draining down a slowly varying substrate, J. Non-Newtonian Fluid Mech. **224**, 30 (2015).
[13] S. D. R. Wilson and S. L. Burgess, The steady, spreading flow of a rivulet of mud, J. Non-Newtonian Fluid Mech. **79**, 77 (1998).
[14] F. H. H. Al Mukahal, B. R. Duffy, and S. K. Wilson, Rivulet flow of generalized Newtonian fluids, Phys. Rev. Fluids **3**, 083302 (2018).
[15] S. Rosenblat, Rivulet flow of a viscoelastic liquid, J. Non-Newtonian Fluid Mech. **13**, 259 (1983).
[16] J.-Y. Park, K. Y. Suh, S.-M. Seo, and H. H. Lee, Anisotropic rupture of polymer strips driven by Rayleigh instability, J. Chem. Phys. **124**, 214710 (2006).
[17] L. Kondic, J. A. Diez, P. D. Rack, Y. Guan, and J. D. Fowlkes, Nanoparticle assembly via the dewetting of patterned thin metal lines: Understanding the instability mechanisms, Phys. Rev. E **79**, 026302 (2009).
[18] G. Hulme, The interpretation of lava flow morphology, Geophys. J. Int. **39**, 361 (1974).
[19] N. Garnier, R. O. Grigoriev, and M. F. Schatz, Optical manipulation of microscale fluid flow, Phys. Rev. Lett. **91**, 054501 (2003).
[20] S. K. Wilson and B. R. Duffy, On the gravity-driven draining of a rivulet of fluid with temperature-dependent viscosity down a uniformly heated or cooled substrate, J. Eng. Math. **42**, 359 (2002).
[21] S. K. Wilson and B. R. Duffy, Strong temperature-dependent-viscosity effects on a rivulet draining down a uniformly heated or cooled slowly varying substrate, Phys. Fluids **15**, 827 (2003).
[22] M. Miesowicz, The three coefficients of viscosity of anisotropic liquids, Nature (London) **158**, 27 (1946).
[23] I. W. Stewart, *The Static and Dynamic Continuum Theory of Liquid Crystals* (Taylor & Francis, London, 2004).
[24] J. R. L. Cousins, A. S. Bhadwal, L. T. Corson, B. R. Duffy, I. C. Sage, C. V. Brown, N. J. Mottram, and S. K. Wilson, Weak-anchoring effects in a thin pinned ridge of nematic liquid crystal, Phys. Rev. E **107**, 034702 (2023).
[25] C. Dascalu, A. L. Alexe-Ionescu, and G. Barbero, Experimental evidence for Ohmic behavior of a 5CB planar cell limited by ITO-electrodes in the DC limit, J. Electroanal. Chem. **767**, 63 (2016).
[26] MATLAB, 9.8.0.1417392 (R2020a) (The MathWorks Inc., Massachusetts, 2022).
[27] C. A. Schneider, W. S. Rasband, and K. W. Eliceiri, NIH Image to ImageJ: 25 years of image analysis, Nat. Methods **9**, 671 (2012).
[28] N. J. Mottram, G. McKay, C. V. Brown, C. T. Russell, I. C. Sage, and C. Tsakonas, Flow-induced delayed Freedericksz transition, Phys. Rev. E **93**, 030701(R) (2016).
[29] B. R. Duffy and H. K. Moffatt, Flow of a viscous trickle on a slowly varying incline, Chem. Eng. J. Biochem. Eng. J. **60**, 141 (1995).
[30] C. Paterson, S. K. Wilson, and B. R. Duffy, Pinning, de-pinning and re-pinning of a slowly varying rivulet, Eur. J. Mech. B: Fluids **41**, 94 (2013).
[31] A. S. Alshaikhi, S. K. Wilson, and B. R. Duffy, Rivulet flow over and through a permeable membrane, Phys. Rev. Fluids **6**, 104003 (2021).
[32] R. V. Craster and O. K. Matar, Dynamics and stability of thin liquid films, Rev. Mod. Phys. **81**, 1131 (2009).
[33] J. R. L. Cousins, B. R. Duffy, S. K. Wilson, N. J. Mottram, and S. K. Wilson, Young and Young–Laplace equations for a static ridge of nematic liquid crystal, and transitions between equilibrium states, Proc. R. Soc. A **478**, 20210849 (2022).
[34] A. Sengupta, *Topological Microfluidics* (Springer, Dordrecht, 2013).
[35] A. S. Bhadwal, Flexoelectricity in Liquid Crystal Materials, Ph.D. thesis, Nottingham Trent University, 2021.
[36] A. Suh, H. Ahn, T. J. Shin, and D. K. Yoon, Controllable liquid crystal defect arrays induced by an in-plane electric field and their lithographic applications, J. Mater. Chem. C **7**, 1713 (2019).

[37] L. T. Corson, N. J. Mottram, B. R. Duffy, S. K. Wilson, C. Tsakonas, and C. V. Brown, Dynamic response of a thin sessile drop of conductive liquid to an abruptly applied or removed electric field, Phys. Rev. E **94**, 043112 (2016).

[38] C. V. Brown, A. M. J. Edwards, A. Roberts, M. I. Newton, I. C. Sage, R. Ledesma-Aguilar, and G. McHale, Bubble control, levitation, and manipulation using dielectrophoresis, Adv. Mater. Interfaces **8**, 2001204 (2021).

[39] http://doi.org/10.5281/zenodo.11276723